Relativistic mean-field description of neutron-deficient platinum isotopes

M. M. Sharma
Science and Engineering Research Council, Daresbury Laboratory, Daresbury, Warrington WA4 4AD, United Kingdom

P. Ring
Physik Department, Technische Universität München, D-8046 Garching, Germany
(Received 11 March 1992)

We have studied neutron-deficient even-mass platinum isotopes in the framework of the relativistic mean-field theory. The ground-state properties of nuclei have been calculated in the $\sigma\omega\rho$ model with the nonlinear scalar self-interaction of the σ meson. The charge radii, binding energies, and deformation properties have been obtained in the relativistic Hartree approximation with deformed basis. Solutions have been obtained for both the prolate as well as oblate shapes. A comparison of the calculated properties has been made with data from recent measurements on these nuclei performed at the ISOLDE project at CERN. It has been shown that the isotopic shift measurements reveal an oblate shape for all even platinum isotopes, in contrast with some existing theoretical calculations which indicate prolate shape for highly neutron-deficient isotopes.

PACS number(s): 21.60.−n, 21.60.Jz, 27.70.+q, 27.80.+w

I. INTRODUCTION

Ground-state properties of nuclei have been a subject of intense study ever since shell-model approaches came into being. Nonrelativistic approaches with Skyrme interactions [1] have long been employed to study spherical as well as deformed nuclei. Only very recently have the relativistic mean-field (RMF) models based on quantum hadrodynamics [2] been used to describe the ground-state properties of nuclei. The charge radii and binding energies of spherical nuclei over the Periodic Table have been excellently reproduced [3]. The relativistic Hartree approach with nonlinear σ interaction has been successful. The parameter set NL1 has, in particular, been very attractive in reproducing the properties of spherical nuclei. A limited, albeit, appropriate description of the properties of deformed nuclei has been obtained.

The platinum isotopes have been a matter of challenge for theoretical calculations. The change of shape from oblate to prolate in going to the more neutron-deficient isotopes presents a suitable test of models. Self-consistent Hartree-Fock plus BCS calculations [4] have been performed in the nonrelativistic approaches using the Skyrme type of interactions and deformation properties of a chain of isotopes in the region of Pt nuclei have been studied. With a view to discern the shape of these nuclei, potential-energy surfaces have been mapped [5]. The calculations have suggested a coexistence of shape in light Pt isotopes. In extensive calculations by Kumar and Baranger [6], a prediction of the change in the ground-state shape in going from light to heavy Pt isotopes has been made. Hartree-Fock-Bogoliubov calculations [7] for Pt isotopes have been carried out and a gradual shape transition from prolate to oblate with an increase in neutron number in Pt nuclei has been implied. Deformation parameters obtained in these and other calculations [4–7] have found appropriate agreement with the measurements of the $B(E2)$ values. There is, however, not much unanimity in the shape of various Pt nuclei predicted by theoretical models, in particular, that of neutron-deficient ones with mass $A=184-190$. In view of recent improved precision in the measurements of nuclear properties, one is led to reconsider the theoretical models once again.

The generator coordinate method has found an appropriate application in the calculations of deformed nuclei. It allows one to obtain the solution in terms of collective variables and mimics the configuration mixing with approximate projection of angular momentum. The method has been applied mostly to s-d shell nuclei and recently it has been employed to study shapes in Hg isotopes [8]. Collective zero-point motion has been suggested to influence the properties of nuclei such as the charge radius and binding energy. It has been surmised that quadrupole correlations in nuclei like Sr induce a decrease of about 2 MeV in total energy [9]. The effect of the zero-point motion on the ground-state charge radii is not clear, but it tends to smoothen the rapid variation in charge radii predicted by the mean-field approach [9].

Experimentally, quadrupole moments of first excited states have been measured [10] in several Pt isotopes indicating an oblate shape for nuclei heavier than $A=190$. Charge radii measurements using laser spectroscopy have become in vogue due to its ability to measure the isotope shifts precisely and thus differentiate the charge radii of various isotopes. This bears upon the shape and deformation of nuclei considered and deformation parameters can be extracted from the charge radii differences. The charge radii themselves, however, do not deliver the signature of the deformation. In order to ascertain the shape of the nuclei, one resorts to comparing the theoretical results with the experimental data. In such a comparison of measurements [11] on charge radii changes of even-mass Pt isotopes with the calculations [4]

with the Skyrme interaction SIII, a possible shape transition near the ^{186}Pt and ^{188}Pt nuclei has been contemplated.

Recently, precision measurements [12] on the magnetic moments, quadrupole moments, and isotope shifts of many platinum isotopes have been performed at the online isotope separator ISOLDE at CERN. The method of resonance ionization mass spectroscopy in conjunction with laser-induced desorption has been applied to measure the hyperfine-structure splitting and isotope shifts with an increased accuracy. The quadrupole deformation parameters have been extracted from the measured isotopic shifts.

In this paper, we present the results of a first detailed study of the ground-state properties of an isotopic chain of deformed heavy nuclei in the framework of the RMF theory. With the recent laser spectroscopic measurements [12] in view, we have calculated the ground-state properties of many even-mass Pt isotopes. Using the RMF theory, we explore the role the nuclear shapes and their deformation play on the observed nuclear properties. In the mean-field approach that we employ, the effect of the angular momentum and particle number projection and of the collective vibrations on the ground-state nuclear properties is not taken into account. It is estimated that these additional features, if incorporated, would increase the total energy of nuclei by only a few MeV. The exact value of such a change is, however, a matter of extensive calculations and is beyond the purview of the present paper. The paper is organized as follows. Section II describes the details of the theoretical formalism employed in the relativistic mean-field treatment of the deformed nuclei. In Sec. III, we provide the details of the calculations. In Sec. IV results of the calculations have been presented. These results have been confronted with the results of the isotopic shift measurements and a discussion has been made with regard to the determination of shape of nuclei. The last section summarizes the conclusions.

II. RELATIVISTIC MEAN-FIELD APPROACH

The RMF theory [2] starts with the interaction of Dirac nucleons with various mesons and electromagnetic field. The corresponding Lagrangian density can be written as

$$\begin{aligned}\mathcal{L}=&\bar{\psi}(i\partial\!\!\!/-M)\psi-\tfrac{1}{2}\partial_\mu\sigma\partial^\mu\sigma-U(\sigma)-\tfrac{1}{4}\Omega_{\mu\nu}\Omega^{\mu\nu}\\&+\tfrac{1}{2}m_\omega^2\omega_\mu\omega^\mu-\tfrac{1}{4}\mathbf{R}_{\mu\nu}\mathbf{R}^{\mu\nu}+\tfrac{1}{2}m_\rho^2\boldsymbol{\rho}_\mu\boldsymbol{\rho}^\mu-\tfrac{1}{4}F_{\mu\nu}F^{\mu\nu}\\&-g_\sigma\bar{\psi}\sigma\psi-g_\omega\bar{\psi}\omega\!\!\!/\psi-g_\rho\bar{\psi}\boldsymbol{\rho}\!\!\!/\boldsymbol{\tau}\psi-e\bar{\psi}\mathbf{A}\!\!\!/\psi\ .\end{aligned}\tag{1}$$

The meson fields taken into account are the isoscalar-scalar σ meson, the isoscalar-vector ω meson, and the isovector-vector ρ meson. The ρ meson provides the necessary isospin asymmetry. The σ-meson potential contains self-interacting nonlinear cubic (σ^3) and quartic (σ^4) terms with strength parameters g_2 and g_3, respectively:

$$U(\sigma)=\tfrac{1}{2}m_\sigma^2\sigma^2+\frac{g_2}{3}\sigma^3+\frac{g_3}{4}\sigma^4\ .\tag{2}$$

The nonlinear coupling of the σ meson provides a necessary ingredient in describing the ground-state properties of the nuclei. It is also required for an appropriate description of the surface properties of the nuclei [13].

The classical variational principle gives the equations of motion which for the stationary states with time-reversal invariance and charge conservation lead to the Dirac equation for the nucleons:

$$\{-i\boldsymbol{\alpha}\nabla+V(\mathbf{r})+\beta[M+S(\mathbf{r})]\}\psi_i=\epsilon_i\psi_i\ ,\tag{3}$$

with the repulsive *vector* potential

$$V(\mathbf{r})=g_\omega\omega_0(\mathbf{r})+g_\rho\tau_3\rho_0(\mathbf{r})+e\frac{1+\tau_3}{2}A_0(\mathbf{r})\ ,\tag{4}$$

and the attractive *scalar* potential

$$S(\mathbf{r})=g_\sigma\sigma(\mathbf{r})\ .\tag{5}$$

The scalar σ field contributes to the effective mass as

$$M^*(\mathbf{r})=M+S(\mathbf{r})\ .\tag{6}$$

The equations for the mesonic fields are time-independent inhomogeneous Klein-Gordon equations with source terms involving the baryon densities

$$\begin{aligned}&\{-\Delta+m_\sigma^2\}\sigma(\mathbf{r})=-g_\sigma\rho_s(\mathbf{r})-g_2\sigma^2(\mathbf{r})-g_3\sigma^3(\mathbf{r})\ ,\\&\{-\Delta+m_\omega^2\}\omega_0(\mathbf{r})=g_\omega\rho_v(\mathbf{r})\ ,\\&\{-\Delta+m_\rho^2\}\rho_0(\mathbf{r})=g_\rho\rho_3(\mathbf{r})\ ,\\&-\Delta A_0(\mathbf{r})=e\rho_c(\mathbf{r})\ .\end{aligned}\tag{7}$$

The corresponding source terms are

$$\begin{aligned}\rho_s&=\sum_{i=1}^{A}\bar{\psi}_i\psi_i\ ,\\\rho_v&=\sum_{i=1}^{A}\psi_i^\dagger\psi_i\ ,\\\rho_3&=\sum_{p=1}^{Z}\psi_p^\dagger\psi_p-\sum_{n=1}^{N}\psi_n^\dagger\psi_n\ ,\\\rho_c&=\sum_{p=1}^{Z}\psi_p^\dagger\psi_p\ ,\end{aligned}\tag{8}$$

where the sums are taken over the valence nucleons only. The present approach neglects the contributions of negative-energy states (*no-sea* approximation).

The Dirac equation is solved using the method [3] based on an expansion in a basis of harmonic-oscillator eigenfunctions of an axially symmetric deformed potential of the form

$$V_{\rm osc}(z,r_\perp)=\tfrac{1}{2}M\omega_z^2z^2+\tfrac{1}{2}M\omega_\perp^2r_\perp^2\ .\tag{9}$$

The basis is defined in terms of the oscillator constant $\hbar\omega_0$ and the deformation parameter β_0, which determine the oscillator frequencies

$$\begin{aligned}\hbar\omega_z&=\hbar\omega_0\exp(-\sqrt{5/4\pi}\beta_0)\ ,\\\hbar\omega_\perp&=\hbar\omega_0\exp(+\tfrac{1}{2}\sqrt{5/4\pi}\beta_0)\ .\end{aligned}\tag{10}$$

The oscillator length parameters are given by

$$b_z=\sqrt{\hbar/M\omega_z}\ ,\quad b_\perp=\sqrt{\hbar/M\omega_\perp}\ , \tag{11}$$

where the volume conservation requires $b_\perp^2 b_z=b_0^3$. The Klein-Gordon equations for mesonic fields are solved similarly by expansion in the deformed oscillator basis with the deformation β_0 and with an oscillator length $b_B=b_0/\sqrt{2}$. The deformation parameter β_2 is obtained from the sum of the calculated quadrupole moment for protons and neutrons using the relationship

$$Q=Q_n+Q_p=\left[\frac{16\pi}{5}\right]^{1/2}\frac{3}{4\pi}AR_0^2\beta_2\ , \tag{12}$$

where $R_0=1.2A^{1/3}$. The basis includes states up to a certain major-shell quantum number N_F for fermions and N_B for bosons for the expansion.

III. DETAILS OF CALCULATIONS

The platinum nuclei considered here are even-mass nuclei with mass number $A=184$ up to $A=198$. All of these isotopes are open-shell nuclei both in protons and neutrons, thus requiring the inclusion of pairing. The latter has been included phenomenologically in the BCS formalism with a constant pairing gap taken from the difference of particle separation energies [14] of neighboring nuclei. The parameter set NL1 has been employed for all nuclei. This set has been found to be very successful for the ground-state properties of many nuclei. It was fitted [15] to reproduce the ground-state properties of light and heavy nuclei including two isotopes of Ca and Sn. For comparison we have also performed calculations with the parameter set NL2. This parameter set has had a limited success [3] in getting the ground-state (g.s.) properties of nuclei. We explore if and how well NL2 works for deformed nuclei considered here and we compare its results with those of NL1. The number of shells taken into account is 12, both for the fermionic (N_F) as well as the bosonic (N_B) expansion. The basis parameters $\hbar\omega$ and β_0 used for the calculations have been taken to be $41A^{-1/3}$ and 0.5, respectively.

In order to understand the departure of Pt nuclei and their properties from the spherical configuration, we also have performed the calculations with spherical basis. For the spherical solutions of the Hartree equations, the expansion is performed for both the fermionic and bosonic basis up to 20 shells.

IV. RESULTS AND DISCUSSION

A. Binding energies

The results of the deformed mean-field calculations with the parameter set NL1 are shown in Table I. Columns 2 and 3 show the binding energy per nucleon of platinum nuclei obtained for the oblate and prolate solutions of the RMF equations, respectively. The binding energy of nuclei obtained by constraining the basis to be spherical are also shown for comparison in the fourth column. It can be seen that the binding of nuclei for the spherical case is considerably smaller than given by the deformed solutions. The last column shows the empirical binding energies from the compilation of Wapstra and Audi [14]. A comparison of the binding energies of both the oblate and prolate solutions with the empirical values in Table I shows that except for the lightest and the heaviest nuclei, the total binding energies are reproduced by the deformed RMF theory within a few MeV. Thus, the parameter set NL1 describes adequately the binding energies of platinum isotopes in axially symmetric configurations.

TABLE I. Binding energy per nucleon (in MeV) of platinum nuclei obtained for oblate, prolate, and spherical solutions in the RMF theory with the parameter set NL1. The empirical binding energies (expt.) are also shown for comparison.

Nucleus	E/A (oblate)	E/A (prolate)	E/A (spherical)	E/A (expt.)
^{184}Pt	−7.978	−7.980	−7.833	−7.943
^{186}Pt	−7.973	−7.975	−7.831	−7.947
^{188}Pt	−7.966	−7.966	−7.826	−7.948
^{190}Pt	−7.963	−7.953	−7.815	−7.947
^{192}Pt	−7.954	−7.940	−7.812	−7.943
^{194}Pt	−7.940	−7.927	−7.810	−7.936
^{196}Pt	−7.922	−7.910	−7.809	−7.927
^{198}Pt	−7.901	−7.888	−7.808	−7.914

It can be noticed from Table I that the binding energies for the prolate and oblate solutions are very close to each other. The differences in the binding energy of the ground state of the oblate and the prolate configuration as given by

$$E_{PO}=E(\text{oblate})-E(\text{prolate})\ , \tag{13}$$

are shown in Fig. 1. The points (circles) joined by a solid line show the behavior of the ground-state energy of the oblate configuration *vis à vis* the prolate one. The closeness in the values of the prolate and oblate ground-state energies is striking for the neutron-deficient isotopes below mass number $A=190$, where the difference in the total energy of nuclei between the two configurations amounts to 500 keV or less. It is consistent with the calculations [5] of the potential-energy surfaces, where a secondary minimum has been found to lie within 0.5 MeV. This is apparently the region of coexistence of shape where the prolate ground state has been predicted at 500 keV or higher than its oblate counterpart. As the figure reveals, the energy of the oblate configuration for most of the isotopes is lower than that of the prolate configuration except for the more neutron-deficient isotopes (^{184}Pt and ^{186}Pt), in which case the binding energy of the prolate configuration is lower than that of the oblate configuration. The difference in the energy between the two configurations increases in going to higher masses. This implies that within the axially symmetric relativistic mean field with the parameter set NL1, the oblate configuration has an energy minimum for most of the platinum isotopes considered here save the two highly neutron-deficient ones.

Table II shows the binding energy per nucleon obtained in the calculations with the parameter set NL2. A

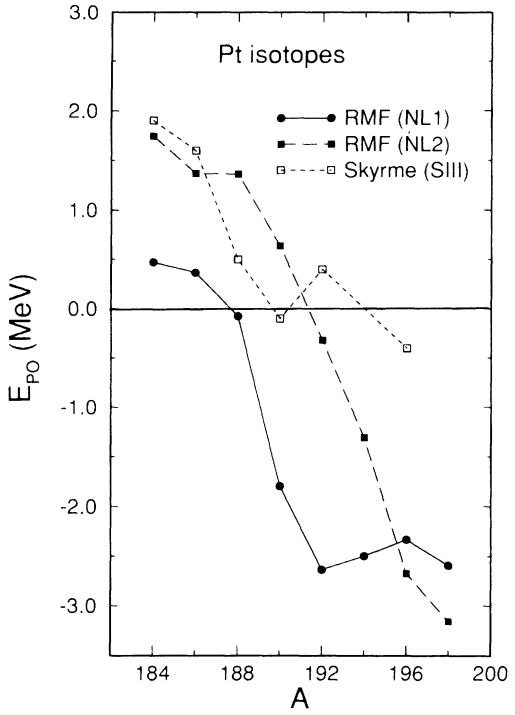

FIG. 1. The energy difference E_{PO} between the oblate and prolate minima obtained in the RMF theory with the parameter sets NL1 and NL2. The values obtained for the self-consistent Hartree-Fock plus BCS calculations [4] with the Skyrme interaction SIII are also shown for comparison.

comparison of the energies of oblate and prolate configurations with the empirical binding energies shows that the set NL2 overestimates the binding of the lightest platinum isotope by 20 MeV. This difference in the prediction of the deformed calculations and the empirical data narrows down in going to higher-mass Pt nuclei and reaching good agreement for ^{194}Pt. As in the case of NL1, the spherical solution for the set NL2 also yields nuclei which are less bound than in reality.

The differences in the energies of the oblate and prolate shapes for NL2 have been plotted in Fig. 1. The curve for NL2 shows that for the four lightest Pt isotopes the prolate configuration has the energy minimum. For ^{192}Pt and heavier isotopes, the oblate configuration has lower energy than the prolate configuration, a trend similar to that with the parameter set NL1. The curve for NL2 is quite parallel to that of NL1, but only a little shifted up in the energy difference E_{PO}. In the case of NL2, the value of E_{PO} for the three lightest Pt isotopes is about 1.5 MeV, in contrast with that predicted by NL1. Thus, NL2 does not seem to follow the shape coexistence in light Pt isotopes correctly. A comparison of the energy difference E_{PO} taken from the results of Skyrme Hartree-Fock calculations [4] with the Skyrme interaction SIII has also been shown in Fig. 1. The data (open squares) show a trend somewhat parallel to that of NL2 for many light isotopes. The Skyrme calculations [4] predict a possible shape transition of the ground state from prolate to oblate at mass 190. For the two lightest isotopes the energy difference E_{PO} is very close to that for NL2. Thus, shape coexistence in light Pt isotopes is not well predicted by the Skyrme force SIII, a case similar to NL2. There is another parallel in the two interactions SIII and NL2. It is on the compressibility of nuclear matter. NL2 has a large compression modulus of 400 MeV as compared to 365 MeV for SIII. These values are much larger than the value of 212 MeV for NL1. It may be noted that while the force SIII has been successful in reproducing the ground-state properties of spherical nuclei, it overestimates the breathing-mode energies of ^{208}Pb and other heavy nuclei by a few MeV, a behavior hardly appropriate for a good interaction.

TABLE II. Binding energy per nucleon (in MeV) of platinum nuclei obtained for oblate, prolate, and spherical solutions in the RMF theory with the parameter set NL2. The empirical binding energies (expt.) are also shown for comparison.

Nucleus	E/A (oblate)	E/A (prolate)	E/A (spherical)	E/A (expt.)
^{184}Pt	−8.053	−8.062	−7.951	−7.943
^{186}Pt	−8.036	−8.044	−7.939	−7.947
^{188}Pt	−8.015	−8.023	−7.923	−7.948
^{190}Pt	−7.996	−7.999	−7.896	−7.947
^{192}Pt	−7.975	−7.972	−7.876	−7.943
^{194}Pt	−7.948	−7.941	−7.860	−7.936
^{196}Pt	−7.917	−7.903	−7.843	−7.927
^{198}Pt	−7.882	−7.866	−7.831	−7.914

B. Deformation

We have shown in Table III the corresponding deformation parameter β_2 obtained from the solution of relativistic deformed Hartree equations with the parameter set NL1 and NL2 for both the oblate as well as prolate shapes. The equilibrium deformation parameters from the minimization are listed in columns 2–5. A comparison of these values, β_2^{ob} and β_2^{pr} for oblate and prolate configurations, respectively, with the β_2 values extracted from the recent isotope shift measurements [12] at the ISOLDE project at CERN, has been shown in Table III. The experimental values $|\beta_2(\mathrm{IS})|$ do not bear any signature as to the determination of the shape of the nucleus. The isotopic-shift measurements yield only the magnitude of the deformation parameter.

The β_2 values deduced from $B(E2)$ values and taken from the recent compilation [16] are also shown in Table III. These values compare very favorably with those derived from the isotope-shift measurements [12]. The β_2 values from oblate solutions for both the parameter sets NL1 and NL2 compare well with the β_2 values from the isotope-shift measurements and with the β_2 values from $B(E2)$ measurements. The deformation parameter ϵ_2 from the parametrization of the mass formula by Möller and Nix (MN) [17] is shown for comparison in the last column of Table III. Though the parameters β_2 and ϵ_2 are not the same, the magnitude of ϵ_2 for axially symmetric shapes is normally 10% lower than the corresponding β_2 value. The two values are thus comparable in magnitude. It may be noted that the parameter ϵ_2 car-

TABLE III. Deformation parameter β_2 obtained from minimization of the relativistic deformed Hartree equations, for both the oblate (β_2^{ob}) as well as the prolate (β_2^{pr}) solutions with the parameter sets NL1 and NL2. The empirical values of β_2 extracted from the recent isotopic-shift (IS) measurements [12] using laser spectroscopy are also shown. The last column shows the parameter ϵ_2 from the parametrization [17] of Möller and Nix (MN).

Nucleus	β_2^{ob} (NL1)	β_2^{pr} (NL1)	β_2^{ob} (NL2)	β_2^{pr} (NL2)	$\lvert\beta_2(\mathrm{IS})\rvert$	$\lvert\beta_2[B(E2)]\rvert$	ϵ_2 (MN)
^{184}Pt	−0.249	0.321	−0.228	0.329	0.21(1)	0.2294(40)	0.225
^{186}Pt	−0.246	0.310	−0.227	0.332	0.20(1)	0.1976(38)	0.217
^{188}Pt	−0.172	0.293	−0.209	0.335	0.18(1)	0.1830(17)	−0.158
^{190}Pt	−0.162	0.242	−0.178	0.330	0.16(1)	0.1490(9)	−0.150
^{192}Pt	−0.156	0.168	−0.165	0.320	0.15(1)	0.1549(24)	−0.150
^{194}Pt	−0.147	0.146	−0.149	0.315	0.143(3)	0.1434(26)	−0.142
^{196}Pt	−0.133	0.127	−0.142	0.149	0.13(1)	0.1308(19)	−0.133
^{198}Pt	−0.113	0.104	−0.115	0.109	0.12(1)	0.1130(27)	−0.133

ries the signature as to indicate the shape of nuclei arising out of the minimization in the mass formula. As indicated, isotopes lighter than ^{188}Pt have been ascribed a prolate shape and the heavier ones, including ^{188}Pt, have acquired an oblate shape.

The theoretically obtained deformation parameters for NL1 have been compared in Fig. 2 with the deformation parameters obtained by Möller and Nix [17]. The circles and squares show the β_2 values obtained in the RMF theory for the prolate and oblate configurations, respectively. The calculated values show the deformation of isotopes up to mass number 204. The calculations for three isotopes heavier than ^{198}Pt were made in order to check the consistency of deformation obtained for these nuclei, as nuclei heavier than 198 would tend to become spherical due to an approaching shell closure for neutrons at mass 204 for platinum. This has indeed been found to be the case as revealed by very small and decreasing deformation for these nuclei in Fig. 2.

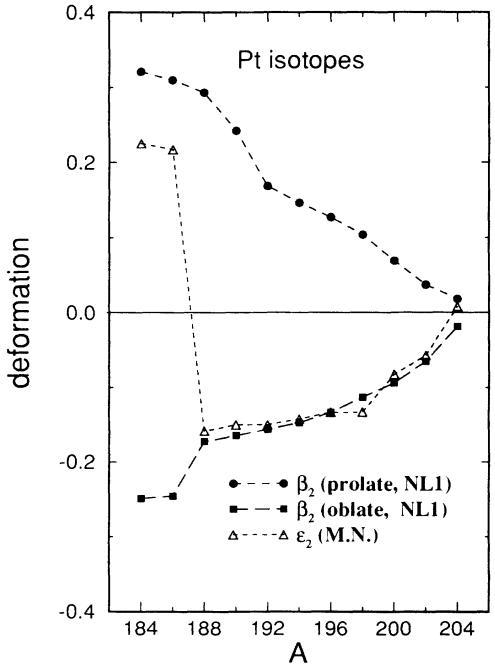

FIG. 2. The deformation parameter β_2 obtained from the solution of relativistic Hartree equations for the oblate and prolate configurations with the parameter set NL1. The parameters ϵ_2 from the parametrization [17] of Möller and Nix (MN) are also shown for the Pt isotopes.

The oblate solutions show a gradual increase of deformation with a decrease in mass number except for the two lightest ones, where there is a rather sudden increase in deformation. An increase in the deformation for the prolate solution is also apparent for the lighter Pt isotopes. The Möller and Nix [17] parametrization (open triangles) shows an abrupt change in shape from oblate to prolate (shape transition) in going to low-mass nuclei. The shape transition in this parametrization occurs near $A=188$. The nucleus with mass number 188, according to the latest parametrization [17], acquires an oblate shape. In the previous version [18] of it by the same authors, this nucleus assumed a prolate shape. This change of shape from prolate to oblate is indeed supported by our calculations, as we shall see further. The deformation parameter β_2 obtained with NL1 for the oblate solution shows an excellent agreement with ϵ_2 values for all nuclei all the way up to the semiclosed-shell nucleus ^{204}Pt, except for the two lightest ones. For the lightest nuclei (^{184}Pt and ^{186}Pt), the ϵ_2 values predict a prolate shape, a feature which would be consistent with the prolate energy minimum for these nuclei with the parameter set NL1 in Fig. 1. This is a region of shape coexistence, whereby the prolate and oblate minima lie very close to each other. Thus, a lower-energy minimum alone would not allow us to ascertain the ground-state shape of the nucleus. We will also look at the corresponding charge radii and charge-radii differences in Sec. IV C.

In Fig. 3, we compare the magnitudes of the theoretical β_2 values obtained with the parameter set NL1 with those derived from the isotope-shift (IS) measurements [12] (shown by squares with error bars). The oblate solution yields the deformation parameter which, *in magnitude,* is in overall agreement with the $|\beta_2(\mathrm{IS})|$ value except for the two lightest isotopes. The prolate solution, on the other hand, describes the deformation of only less neutron-deficient isotopes ($A>190$) appropriately. For the more neutron-deficient ones, the prolate solution yields much larger deformation and the disagreement is highest for the isotopes with $A<192$.

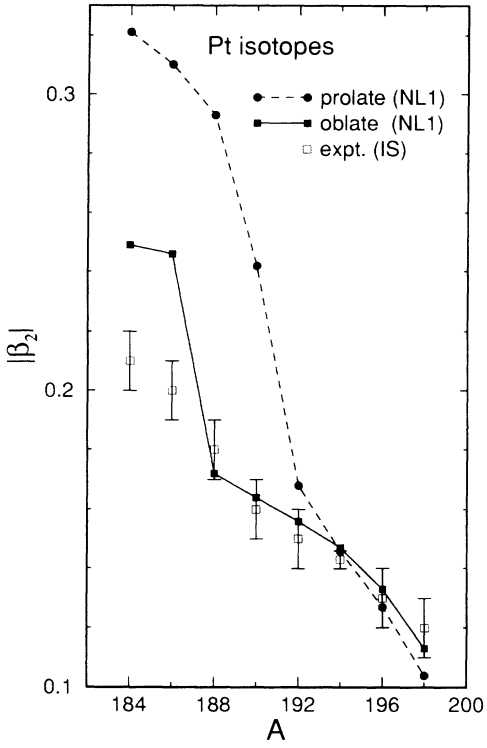

FIG. 3. Magnitude of the deformation β_2 for the oblate and prolate configurations with the parameter set NL1 compared with the deformation obtained from the isotope-shift measurements [12].

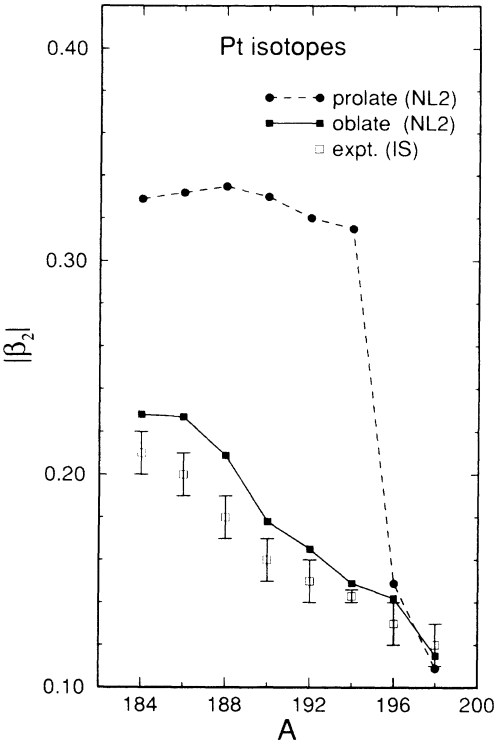

FIG. 5. Magnitude of the deformation parameter β_2 for the parameter set NL2. For details, see the caption of Fig. 3.

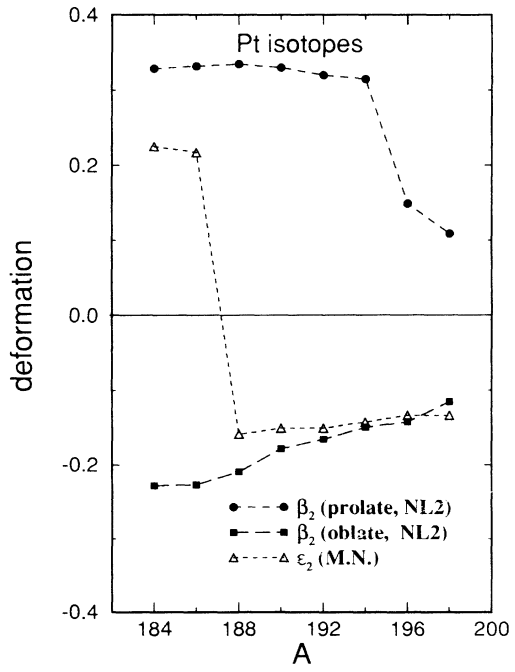

FIG. 4. The deformation parameters for the set NL2. For details, refer to the caption of Fig. 2.

The deformation parameters obtained with the parameter set NL2 have been compared in Fig. 4 with the ϵ_2 values. Again, the oblate solution shows a gradual increase in deformation in going to the lighter nuclei. The prolate solution, on the other hand, indicates an abrupt increase in deformation below mass number $A = 196$. The ϵ_2 values shown in the figure agree well with the values of deformation from the oblate solution, though the ϵ_2 values favor a shape transition as illustrated by the dots joining the data. The magnitudes of deformation parameters for the set NL2 have been shown in Fig. 5. That the magnitude of the β_2 values obtained within the oblate solution shows an overall agreement with the $|\beta_2|$ values derived from the isotope-shift measurements (shown with error bars) is demonstrated clearly in this figure. The prolate solution, in contrast, overestimates the magnitude of the deformation for all isotopes except for the heaviest ones, i.e., ^{196}Pt and ^{198}Pt. This behavior of the prolate solution with NL2 is very similar to that of NL1 as shown in Fig. 3. It may be pointed out again that just on the basis of a comparison of the magnitudes of deformations with the deformations obtained in the RMF theory, one would not be able to ascribe a particular shape to the Pt nuclei.

C. Charge radii

Charge radii and charge radii differences are crucial to the study of any systematic change in shape of nuclei as charge radii can be measured with considerable precision using the laser spectroscopic technique. Charge radii are

TABLE IV. Change in charge radii (isotope shift) $\delta\langle r^2\rangle^{194,A}$ of platinum isotopes with mass number A obtained from the solution of relativistic Hartree equations in oblate, prolate, and spherical basis with the parameter set NL1. The experimental values [12] obtained from resonance ionization mass spectroscopy at the ISOLDE project at CERN have also been shown in the last column. The nucleus with mass $A=194$ has been taken as a reference.

Nucleus	$\delta\langle r^2\rangle^{194,A}_{\text{oblate}}$	$\delta\langle r^2\rangle^{194,A}_{\text{prolate}}$	$\delta\langle r^2\rangle^{194,A}_{\text{spherical}}$	$\delta\langle r^2\rangle^{194,A}_{\text{expt.}}$
^{184}Pt	−0.147	0.197	−0.637	−0.232
^{186}Pt	−0.034	0.291	−0.498	−0.207
^{188}Pt	−0.313	0.345	−0.373	−0.188
^{190}Pt	−0.196	0.185	−0.247	−0.134
^{192}Pt	−0.093	−0.046	−0.124	−0.072
^{194}Pt	0.000	0.000	0.000	0.000
^{196}Pt	0.085	0.064	0.120	0.074
^{198}Pt	0.133	0.088	0.247	0.151

usually obtained by folding the finite size of the protons in the proton distribution of the nuclei. There are few other effects which might influence the rms charge radius of the nuclei. These effects are the center-of-mass projection, the angular momentum, the particle number projection, and the zero-point motion. Some of these effects have been considered in nonrelativistic general coordinate method calculations [9]. Relativistic approaches do not at present take these effects into account. In nonrelativistic calculations, these effects are often very small. In the present calculations, we ignore these effects and calculate charge radii in the pure mean-field approximation. In Tables IV and V, we show the change in the charge radii (isotope shift), $\delta\langle r^2\rangle^{194,A}$, of platinum isotopes with mass number A as defined by

$$\delta\langle r^2\rangle^{194,A}=\langle r^2\rangle^{A}-\langle r^2\rangle^{194}\ . \tag{14}$$

In Table IV we compare the results of the parameter set NL1 with the empirical data. The first three columns show the values obtained in the RMF theory for the oblate, prolate, and spherical configurations. The spherical calculations were performed with a spherical basis as discussed in Sec. III. The nucleus with mass $A=194$ has been taken as a reference in order to conform to the values extracted from the isotope-shift measurements. The latter have been shown in the last column of the table. Various values of $\delta\langle r^2\rangle$ have been displayed in Fig. 6 for the set NL1. First, we consider the empirical values (experiment) of $\delta\langle r^2\rangle$. The values (indicated by diamonds) show a smooth trend with an increase in neutron number. Thus, the empirical charge radius of Pt nuclei increases smoothly with a successive addition of neutrons. The curve shown by a solid line joining the experimental points (diamonds) in Fig. 6 crosses the zero unequivocally. The theoretical points for the prolate configuration, in contrast, exhibit a dramatic trend. In this case, the change in the rms charge radius for nuclei above mass 190 is smooth. For nuclei lighter than and including ^{190}Pt, the $\delta\langle r^2\rangle$ values are positive. This implies that for these (lighter) platinum isotopes, even with a reduction in neutron number, the charge radius is larger than the reference nucleus ^{194}Pt, in complete contradiction to the empirical behavior. The deformation of these prolate configurations from Table III is correspondingly large as compared to the heavier isotopes. Thus, with the parameter set NL1 the behavior of the prolate configuration for the lighter Pt isotopes is at odds with that of the empirical isotope shifts.

The predictions of the oblate configuration for the isotope shifts for the parameter set NL1 are shown in Fig. 6 by squares. The overall trend of $\delta\langle r^2\rangle$ for the oblate shape, including the change in sign, is consistent with the empirical data down to mass number 188. Only for the two lightest isotopes (^{184}Pt and ^{186}Pt) is there a reduction in the charge radius as compared to its heavier neighbors. In magnitude the $\delta\langle r^2\rangle$ values of these nuclei differ slightly from the empirical values. The signature of $\delta\langle r^2\rangle$ for oblate configuration of these nuclei is, however, still the same as that of the empirical values and is in contrast with that of the prolate configuration. The data points (triangles) for the spherical shape of the nuclei in Fig. 6 show a regular and smooth trend in $\delta\langle r^2\rangle$ values

TABLE V. Change in charge radii (isotope shift) $\delta\langle r^2\rangle^{194,A}$ of platinum isotopes obtained with the parameter set NL2. For details refer to the caption of Table IV.

Nucleus	$\delta\langle r^2\rangle^{194,A}_{\text{oblate}}$	$\delta\langle r^2\rangle^{194,A}_{\text{prolate}}$	$\delta\langle r^2\rangle^{194,A}_{\text{spherical}}$	$\delta\langle r^2\rangle^{194,A}_{\text{expt.}}$
^{184}Pt	−0.254	−0.678	−0.627	−0.232
^{186}Pt	−0.127	−0.517	−0.500	−0.207
^{188}Pt	−0.102	−0.347	−0.373	−0.188
^{190}Pt	−0.132	−0.220	−0.248	−0.134
^{192}Pt	−0.062	−0.124	−0.123	−0.072
^{194}Pt	0.000	0.000	0.000	0.000
^{196}Pt	0.105	−0.731	0.123	0.074
^{198}Pt	0.157	−0.766	0.239	0.151

on putting additional neutrons in the nuclei. It shows the extent of deviations of oblate and prolate configurations, respectively, from its spherical counterpart. It may be noticed from Fig. 6 that the empirical values lie close to the spherical values for many heavy Pt isotopes. This is also the region where the actual deformation of nuclei is small. For very neutron-deficient isotopes, the deviations from the spherical configuration are large and the corresponding deformations increase as evidenced by Table III.

It may be mentioned that in Fig. 6, the nucleus ^{194}Pt serves as a reference point for all the data. The charge radii of this nucleus for the oblate, prolate, and spherical configurations are all slightly different from each other. Thus, in order to avoid inconsistencies in the comparison of all the data in Fig. 6, we normalize the charge radii with respect to the nucleus ^{198}Pt. Since this nucleus is much less deformed and is close to being spherical, the values of charge radii obtained for the oblate, prolate, and spherical configurations have been found to converge. Figure 7 shows the values of various theoretical charge radii along with the empirical charge radii normalized to the nucleus ^{198}Pt. The spherical configuration shows a regular increase with mass number as expected. It can be seen that the charge radii for both the oblate and the prolate configurations for nuclei above mass 192 exhibit a close similarity in the values with the empirical ones. The small value of deformation for the nuclei ^{194}Pt, ^{196}Pt, and ^{198}Pt in both the prolate and oblate solutions for NL1 brings the close similarity in their charge radii for prolate and oblate shapes. It is, however, known on the basis of measurements that these nuclei have a well-defined oblate ground state.

In the mass region below $A=192$, the prolate configuration yields charge radii which are drastically different from the empirical ones. Only the oblate solution gives charge radii which are in the vicinity of the empirical values. The nucleus ^{186}Pt shows a charge radius for the oblate configuration, which is larger than the empirical value and is much smaller than the corresponding value for the prolate configuration. This region marks a possible deviation from oblate shape in the direction of a possible triaxiality. The shape of these light nuclei, however, still remains of the oblate type within the confines of the axially symmetric relativistic mean field with the parameter set NL1.

The charge radii obtained with the parameter set NL2 have been displayed in Fig. 8. The normalization of the experimental data from the isotope-shift measurements has been done with respect to the nucleus ^{198}Pt as in Fig.

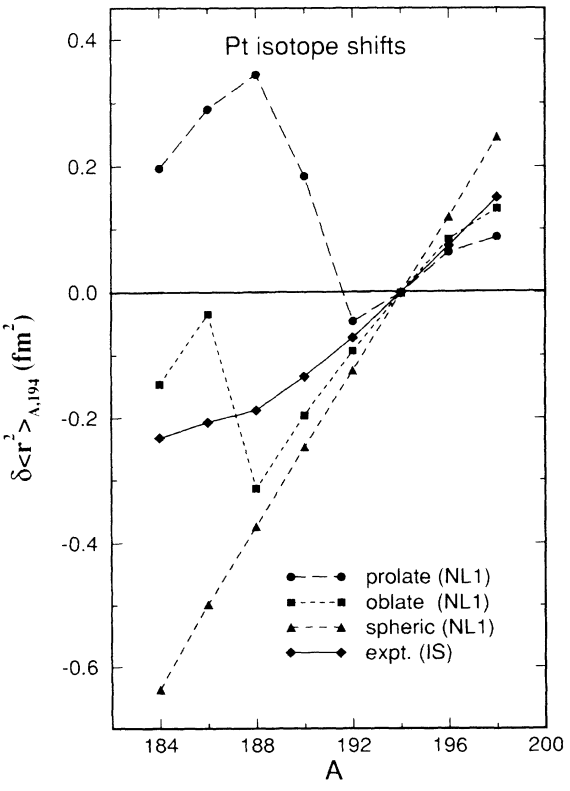

FIG. 6. The change in charge radii for Pt nuclei obtained for the oblate, prolate, and spherical configurations in the RMF theory with the parameter set NL1. The empirical values from the isotope-shift measurements [12] are shown with a solid line. The nucleus ^{194}Pt serves as a reference point for the difference.

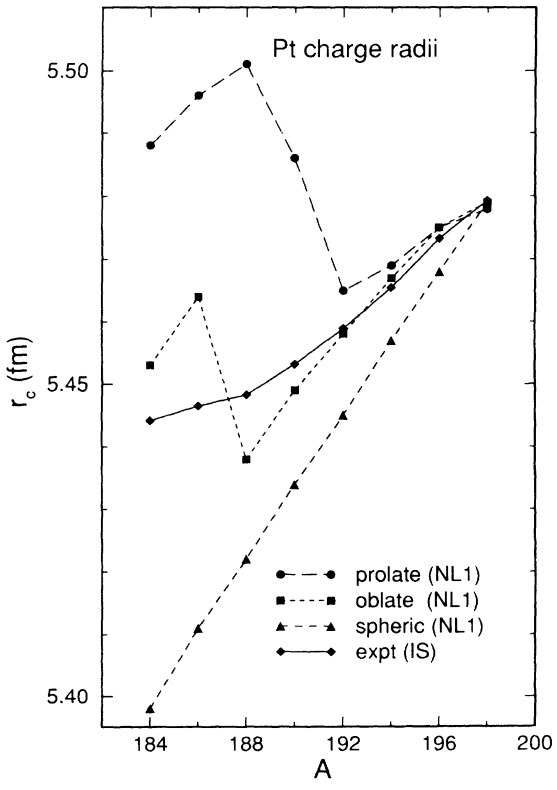

FIG. 7. The charge radii for the Pt isotopes obtained for the oblate, prolate, and spherical configurations in the RMF theory with the parameter set NL1. The empirical values shown have been obtained by normalizing charge radii differences [12] from Fig. 6 with respect to the theoretical charge radius of the nucleus ^{198}Pt. The charge radius of this nucleus for all the three configurations has been found to coincide.

7. The behavior of NL2 in respect of the charge radii for this isotope in the deformed case is different from that in the spherical case as indicated by different charge radii for the deformed (oblate and prolate having same charge radii for ^{198}Pt) and the spherical configurations. The charge radii for the spherical configuration for NL2 are, in general, more distanced from the empirical values as compared to that for NL1 in Fig. 7. NL2, on the other hand, predicts charge radii for the oblate configuration, which show an overall agreement with the empirical charge radii. The prolate configuration, in contrast, yields charge radii which are much larger than the empirical ones. Thus, NL2 favors an oblate shape for all the Pt isotopes, a behavior similar to that of NL1.

As discussed previously, charge radii data on nuclei can be measured precisely using various techniques. There is, however, little empirical knowledge on neutron and thus matter radii of nuclei [19]. Most of the information about neutron and matter radii comes indirectly from analysis of heavy-ion scattering using optical potential. Recently, we have analyzed and compared the neutron-skin thickness of various spherical nuclei in the relativistic mean-field theory and nonrelativistic Skyrme

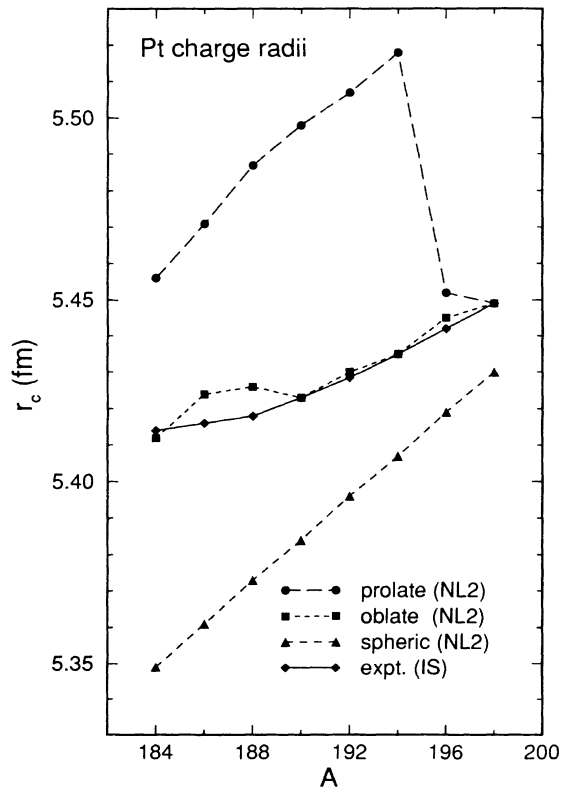

FIG. 8. The charge radii of Pt isotopes for the oblate, prolate, and spherical configurations with the parameter set NL2. The empirical values from IS measurements [12] have been normalized with respect to the theoretical charge radius of the nucleus ^{198}Pt as in Fig. 7. The charge radius for the deformed configurations, where the charge radius has been found to coincide for both the oblate and prolate cases, serves as a reference point.

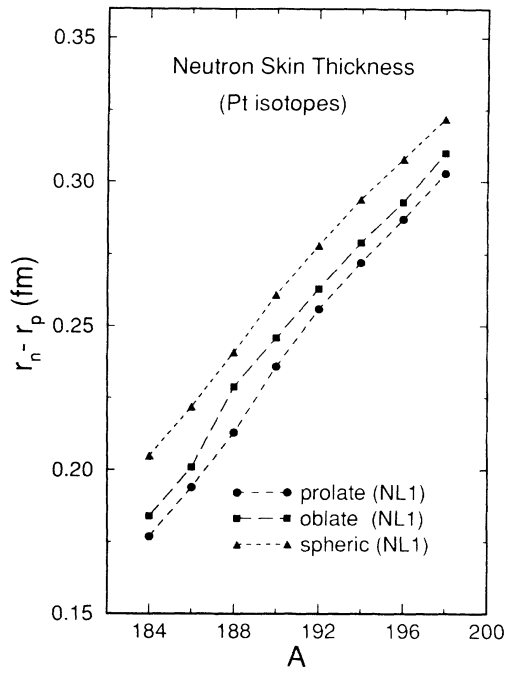

FIG. 9. Neutron-skin thickness of Pt nuclei in the RMF theory with the parameter set NL1 for oblate, prolate, and spherical solutions.

interactions [20]. It has been shown that the response of neutron-skin thickness to the RMF is slightly different than to the Skyrme mean field. In the deformed and spherical relativistic Hartree calculations as discussed in this paper, we show the neutron-skin thickness $(r_n - r_p)$ obtained in the RMF theory for the Pt isotopes in Figs. 9

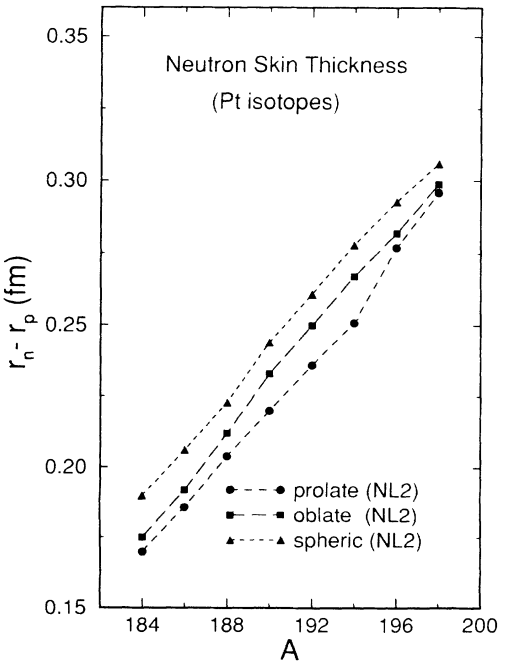

FIG. 10. The same as in Fig. 9 for the parameter set NL2.

and 10 for the parameter sets NL1 and NL2, respectively. Naturally, the neutron-skin thickness increases with addition of neutrons for all three configurations. Evidently, the calculations in the spherical basis provide the largest neutron-skin thickness of all the configurations. Of the deformed ones, the oblate shape yields larger thickness than the prolate shape. This behavior of neutron-skin thickness seems to be similar for both the parameter sets NL1 and NL2. It will be interesting to compare these neutron-skin thicknesses with those obtained with deformed Skyrme calculations.

V. CONCLUSIONS

Relativistic mean-field theory has been applied to study the nuclear ground-state properties of deformed nuclei. The calculations have performed for a chain of neutron-deficient Pt isotopes. The binding energies, deformation parameters, and charge radii have been obtained with the parameter sets NL1 and NL2. A comparison of the theoretical isotope shifts for both the parameter sets NL1 and NL2 with the isotope shifts from the recent precision measurements shows that an oblate shape in the RMF theory is compatible with the empirical isotope shifts for all Pt nuclei including those lighter than mass 190. The magnitude of deformation for oblate configuration for these nuclei is consistent with those extracted from the IS measurements and from $B(E2)$ values. The prolate configuration, on the other hand, yields isotope shifts in charge radii that are drastically incompatible with the empirical measurements. The prolate configuration also assumes a large deformation for these nuclei, which is inconsistent with the deformations provided by the experimental data. Thus, an oblate shape is favored by the relativistic mean field within the axially symmetric domain for all the Pt isotopes considered here. This contrasts with some of the existing nonrelativistic theories where a shape transition to prolate configuration for the lighter Pt isotopes has been predicted.

ACKNOWLEDGMENTS

We would like to thank Ray Nix for fruitful communications. One of the authors (M.M.S.) would like to thank John Lilley for encouragement. This work is supported in part by the Bundesminsterium für Forschung und Technologie, Germany.

[1] P. Quentin and H. Flocard, Annu. Rev. Nucl. Part. Sci. **28**, 523 (1978).
[2] B. D. Serot and J. D. Walecka, Adv. Nucl. Phys. **16**, 1 (1986).
[3] Y. K. Gambhir, P. Ring, and A. Thimet, Ann. Phys. (N.Y.) **511**, 129 (1990).
[4] J. Sauvage-Letessier, P. Quentin, and H. Flocard, Nucl. Phys. A **370**, 231 (1981).
[5] R. Bengtsson, T. Bengtsson, J. Dudek, G. Leander, W. Nazarewicz, and J.-Y. Zhang, Phys. Lett. **183B**, 1 (1987).
[6] M. Baranger and K. Kumar, Nucl. Phys. A **110**, 410 (1968); **122**, 241 (1968).
[7] A. Ansari, Phys. Rev. C **38**, 953 (1988).
[8] P. Bonche, J. Dobaczewski, H. Flocard, P.-H. Heenen, and J. Meyer, Nucl. Phys. A **510**, 466 (1990).
[9] P. Bonche, J. Dobaczewski, H. Flocard, and P.-H. Heenen, Nucl. Phys. A **530**, 149 (1991).
[10] G. J. Gyapong, R. H. Spear, M. P. Fewell, A. M. Baxter, and S. M. Burnett, Nucl. Phys. A **470**, 415 (1987); G. J. Gyapong, R. H. Spear, M. T. Esat, M. P. Fewell, A. M. Baxter, and S. M. Burnett, *ibid.* **458**, 165 (1986).
[11] J. K. P. Lee, G. Savard, J. E. Crawford, G. Thekkadath, H. T. Duong, J. Pinard, S. Liberman, F. Le Blanc, P. Kilcher, J. Obert, J. Oms, J. C. Putaux, B. Roussiere, and J. Sauvage, Phys. Rev. C **38**, 2985 (1988).
[12] T. Hilberath, S. Becker, G. Bollen, H.-J. Kluge, U. Krönert, G. Passler, J. Rikovska, R. Wyss, and the ISOLDE Collaboration, Z. Phys. A **342**, 1 (1992); H.-J. Kluge (private communication).
[13] J. Boguta and A. R. Bodmer, Nucl. Phys. A **292**, 413 (1977).
[14] A. H. Wapstra and G. Audi, Nucl. Phys. A **432**, 1 (1985).
[15] P. G. Reinhard, M. Rufa, J. Maruhn, W. Greiner, and J. Friedrich, Z. Phys. A **323**, 13 (1986); P. G. Reinhard, Rep. Prog. Phys. **52**, 439 (1989).
[16] S. Raman, C. H. Malarkey, W. T. Milner, C. W. Neston, Jr., and P. H. Stelson, At. Data Nucl. Data Tables **36**, 1 (1987).
[17] P. Möller, J. R. Nix, W. D. Myers, and W. J. Swiatecki, At. Data Nucl. Data Tables (to be published); J. R. Nix (private communication).
[18] P. Möller and J. R. Nix, At. Data Nucl. Data Tables **26**, 165 (1981).
[19] C. J. Batty, E. Friedman, H. J. Gils, and H. Rebel, Adv. Nucl. Phys. **19**, 1 (1989).
[20] M. M. Sharma and P. Ring, Phys. Rev. C **45**, 2514 (1992).